Energy deposition of multi-MeV protons in compressed targets of fast-ignition inertial confinement fusion

M. Mahdavi* and T. Koohrokhi†

Department of Physics, Faculty of Basic science, Mazandaran University, P.O. Box 47415-416, Babolsar, Iran

(Received 11 July 2011; revised manuscript received 9 October 2011; published 24 January 2012)

The energy loss and penetration of multi-megelectronvolt protons into a uniform deuterium-tritium (DT) plasma has been calculated. The effects of nuclear elastic scattering and Coulomb interactions are treated from a unified point of view. In general, multiple scattering enhances the proton linear-energy transfer along the initial proton direction, thus the energy deposition increases near the end of its range. The net effect of multiple scattering is to reduce the penetration from 1.20 to 1.02 g cm^{-2} for 12 MeV protons in a $\rho = 500$ g cm^{-3} plasma at $T = 5$ keV. These results should have relevance to proton fast ignition, specifically to energy deposition calculations that critically assess quantitative ignition requirements.

DOI: 10.1103/PhysRevE.85.016405 PACS number(s): 52.25.Fi, 52.25.Dg

I. INTRODUCTION

Fast ignition (FI) of thermonuclear fusion is an attractive scheme to increase the energy gain, reduce the laser driver energy, and relax fuel compression uniformity in inertial confinement fusion [1,2]. In the original scheme, relativistic laser-accelerated electron beams have been proposed to fast ignite the precompressed fuel [2]. These electrons are accelerated by an ultra-intense laser which penetrates through the plasma corona up to the critical density. However, the relativistic electron beam approach suffers problems with localized energy deposition and focusing.

Recently, it has been found that an ultra-intense laser allows the acceleration of protons or even the heavier ions [3,4]. Snavely *et al.* showed that protons with Maxwellian energy distribution are efficiently accelerated by an ultra-intense laser [5]. Following that, Roth *et al.* proposed the use of such a laser-accelerated proton beam as a secondary driver for the fast ignition phase [6]. Because of their highest charge-to-mass ratio, protons do have several advantages compared with other ion species and electrons. They can be accelerated most efficiently up to the highest energies. They can penetrate deeper into a target to reach the high density region, where the hot spot is to be formed because of the quadratic dependence of the stopping power on the charge state. And finally they do, like all ions, exhibit a maximum characteristic of the energy deposition at the end of their range (Bragg peak), which is desirable to heat a localized volume efficiently. Laser-generated protons are characterized by a small source, high degree of collimation, and short duration, which has also been used in proton radiography [7].

The successful realization of fast ignition requires the understanding and control of the transport and energy deposition of proton beams in the target. The penetration depth of a proton beam in a dense plasma is a quantity of particular relevance to fast ignition since it is related to the depth of the region heated by the beam. In the original work introducing the general concepts of FI, the range for ~MeV electrons in core plasmas was estimated based on the stopping power model. Later on, the stopping of fast electrons as well as their multiple scattering of target ions was properly treated [8]. This was further improved and extended by adding the equally significant multiple scattering contribution of target electrons with the help of the multiple scattering theory [9–12]. These works motivate us to use the multiple scattering theory to evaluate the energy deposition of proton beams. Nevertheless, there are differences between electron and proton stopping and the scattering mechanism. In the relativistic electron scheme, the electrons and ions of the target are assumed to be stationary. This assumption is no longer appropriate for proton beams. Furthermore, in the plasmas, nuclear elastic scattering contributes to scattering and slowing down of protons [13]. Recent studies pointed out the possibility of compressing a D/T capsule and generating a blob with a density of $\rho = 300$–500 (g/cm^3),temperature $T = 5$–10 keV and areal density $\rho R = 1$–2 (g/cm^2), using relatively modest laser energy [14–17]. In this paper, we consider laser-accelerated proton beams generated in close proximity to the compressed fuel pellet to provide the ignition spark. Thus, by using the multiple scattering theory, the energy deposition of multi-megaelectron volt protons in compressed targets of fast ignition is calculated in the ignition conditions.

This paper is organized as follows. Section II introduces the differential scattering cross section and stopping power for megaelectron volt protons in plasmas. The multiple scattering theory, which links proton energy loss with range and penetration depth, is presented in Sec. III. Section IV discusses some fundamental results of these calculations.

II. DIFFERENTIAL SCATTERING CROSS SECTION AND STOPPING POWER

Measured differential elastic scattering cross sections for protons on nuclei include the Coulomb scattering component, the nuclear scattering component, and a component representing interference between these two processes. The Coulomb cross section is analytic, and can be subtracted from the total scattering cross section to yield what we call the nuclear plus interference (NI) cross section. The elastic differential

*m.mahdavi@umz.ac.ir
†T.koohrokhi@umz.ac.ir

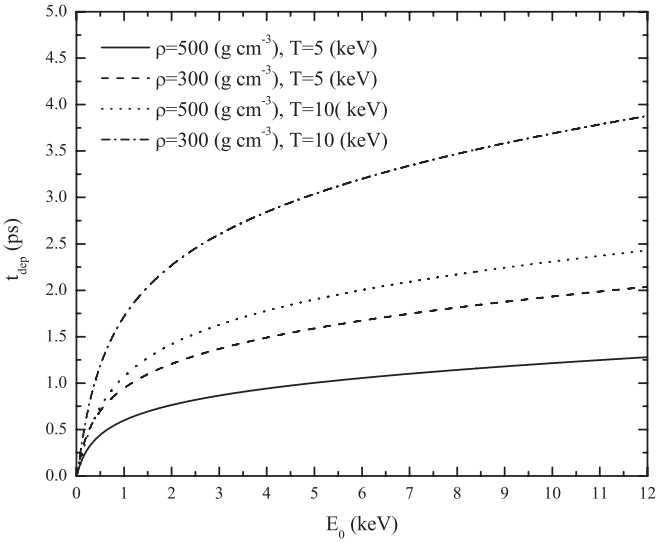

FIG. 1. The proton stopping time $t_{\rm dep}$ in a uniform D/T plasma versus initial proton energy E_0.

Coulomb cross section is the well-known Rutherford's cross section, which in the center-of-mass system is

$$\frac{d\sigma_{pb}^{\rm Coul}}{d\Omega} = \frac{Z_p^2 Z_b^2 e^4}{m_{pb}^2 v_{pb}^4 (1-\mu)^2}. \tag{1}$$

The form of the differential NI cross section is suggested as the exact polynomial expansion [18]

$$\frac{d\sigma_{pb}^{NI}}{d\Omega} = -\frac{2\eta_{pb}}{1-\mu}{\rm Re}\left\{\exp\left(i\eta_{pb}\ln\left(\frac{1-\mu}{2}\right)\right) \times \sum_{l=0}^{l_{\rm max}} \frac{2l+1}{2} a_l P_l(\mu)\right\} + \sum_{l=0}^{2l_{\rm max}} \frac{2l+1}{2} b_l P_l(\mu), \tag{2}$$

which is truncated at the highest-order partial waves $l_{\rm max}$ that contribute to nuclear scattering. The dependence on the relative velocity $v_{pb} = |\mathbf{v}_p - \mathbf{v}_b|$ enters through the expansion coefficients and through the Coulomb parameter, which is defined as $\eta_{pb} = Z_p Z_b e^2/\hbar v_{pb}$, while the dependence on $\mu = \cos\Theta$ is explicit in Eq. (2), where Θ is the scattering angle in the center-of-mass system (Fig. 1). $Z_p e$ and $Z_b e$ are the charges of projectile p and background plasma species b, respectively, and $m_{pb} = m_p m_b/(m_p + m_b)$ is the reduced mass.

The complete treatment of the stopping power of charged particles in plasma was evaluated in pervious work [13]. The stopping power of a projectile due to NI elastic scattering is given by

$$\frac{dE^{NI}}{ds} = -\frac{1}{v_p}\sum_b \int \frac{d^3\mathbf{p}_b}{(2\pi\hbar)^3} f_b(\mathbf{p}_b) m_{pb} v_{pb} \int d\Omega \left(\frac{d\sigma_{pb}^{NI}}{d\Omega}\right) \times \left\{\left(\frac{m_{pb} v_{pb}^2}{m_p} - \mathbf{v}_p.\mathbf{v}_{pb}\right)(1-\cos\Theta) + v_p v_b \sin\psi \sin\Theta\right\}, \tag{3}$$

where ψ is the angle between velocities $\mathbf{v}_p$ and $\mathbf{v}_b$, and Θ is the scattering angle in center-of-mass system.

The usual method for obtaining the stopping power for a charged particle by Coulomb interactions, moving through matter is to divide the calculation into two parts: the long-distance collective excitations and the short-distance hard collisions. Collective effects are important in the long-distance part, and it is evaluated from the j.E power loss of a particle moving in a dielectric medium. The hard collisions are described by Coulomb scattering.

A completely rigorous first-principles calculation of the charged particle stopping power has recently been performed by Brown, Preston, and Singleton (BPS) [19]. This calculation is in exact to leading and next-to-leading order in the plasma number density, including an exact treatment of two-body quantum scattering. No restriction is made on the charge, mass, or speed of this particle. It is, however, assumed that the plasma is not strongly coupled in the sense that the dimensionless plasma coupling parameter $g = e^2 k_D/T$ is small, where k_D is the Debye wave number of the plasma. For example, one finds $g \simeq 0.00846$ for a D/T plasma with density $\rho = 500$ g/cm^3 and temperature $T = 5$ keV. It is shown that plasma quantities always expand in integer powers of the coupling g, and therefore g is the appropriate parameter in which to perform a controlled perturbative analysis for weakly coupled plasmas. The BPS calculation is therefore extremely accurate in the plasma regime realized during the ignition and burn of an inertial confinement fusion capsule. The BPS stopping power of nonrelativistic particles moving through a highly ionized plasma for Coulomb interactions is

$$\frac{dE^{\rm Coul}}{ds} = \sum_b \left(\frac{dE_{b,S}^C}{ds} + \frac{dE_{b,R}^<}{ds} + \frac{dE_b^Q}{ds}\right). \tag{4}$$

The well-known Lenard-Balescu kinetic equation describes the long-distance collective excitations of the plasma [20,21], whereas the Boltzmann equation for pure Coulomb scattering describes the short-distance hard collisions of the plasma particles. A complete description of the plasma includes both the long- and short-distance physics encoded in the Lenard-Balescu and Boltzmann equations, so that the short-distance quantum effects is added to the classical results [22]. The first term of Eq. (4) arises from classical short distance physics

$$\frac{dE_{b,S}^C}{ds} = \frac{Z_p^2 e^2 k_b^2}{m_p v_p}\left(\frac{m_b}{2\pi\beta_b}\right)^{1/2}\int_0^1 du\, u^{1/2}\exp\left(-\frac{1}{2}\beta_b m_b v_p^2 u\right) \times \left\{\left[-\ln\left(\beta_b m_b \frac{Z_p Z_b e^2 K}{m_{pb}}\frac{u}{1-u}\right) + 2 - 2\gamma\right] \times \left[\beta_b M_{pb} v_p^2 - \frac{1}{u}\right] + \frac{2}{u}\right\}, \tag{5}$$

where $M_{pb} = m_p + m_b$ is the total mass of the projectile and plasma particles, $\beta_b = T_b^{-1}$ is the inverse temperature, and $\gamma \simeq 0.57721\ldots$ is Euler's constant. The second term of Eq. (4) related to the long-distance physics

$$\frac{dE_{b,R}^<}{ds} = Z_p^2 e^2 \frac{i}{2\pi}\int_{-1}^1 d\cos\theta\cos\theta \frac{\rho_b(v_p\cos\theta)}{\rho_{\rm total}(v_p\cos\theta)} \times F(v_p\cos\theta)\ln\left(\frac{F(v_p\cos\theta)}{K^2}\right)$$

$$- Z_p^2 e^2 \frac{i}{2\pi} \frac{1}{\beta_b m_p v_p^2} \frac{\rho_b(v_p)}{\rho_{\text{total}}(v_p)} \times \left[F(v_p) \ln\left(\frac{F(v_p)}{K^2}\right) F^*(v_p) \ln\left(\frac{F^*(v_p)}{K^2}\right) \right], \quad (6)$$

where K is an arbitrary wave number so that the total result does not depend on K. However, sometimes choosing K to be a suitable multiple of the Debye wave number of the plasma simplifies the formula. Debye wave number k_b of this species is defined by

$$k_b^2 = 4\pi\beta_b Z_b^2 e^2 n_b, \quad (7)$$

where n_b is the number density of species b. The total Debye wave number k_D is defined by

$$k_D^2 = \sum_b k_b^2. \quad (8)$$

The function $F(u)$ is related to the leading-order plasma dielectric susceptibility that may be expressed in the dispersion form

$$F(u) = -\int_{-\infty}^{\infty} dv \frac{\rho_{\text{total}}(v)}{u - v + i\eta}. \quad (9)$$

The spectral weight $\rho_{\text{total}}(v)$ is defined by

$$\rho_{\text{total}}(v) = \sum_b \rho_b(v), \quad (10)$$

where

$$\rho_b(v) = k_b^2 v \sqrt{\frac{\beta_b m_b}{2\pi}} \exp\left(-\frac{1}{2}\beta_b m_b v^2\right). \quad (11)$$

The third term in Eq. (4) is the short-distance two-body quantum correction to the classical result

$$\frac{dE_b^Q}{ds} = \frac{Z_p^2 e^2 k_b^2}{2\beta_b m_p v_p^2} \left(\frac{\beta_b m_b}{2\pi}\right)^{1/2} \int_0^\infty dv_{pb} \times \left\{ \left[1 + \frac{M_{pb}}{m_b} \frac{v_p}{v_{pb}} \left(\frac{1}{\beta_b m_b v_p v_{pb}} - 1 \right) \right] \times \exp\left(-\frac{1}{2}\beta_b m_b (v_p - v_{pb})^2\right) - \left[1 + \frac{M_{pb}}{m_b} \frac{v_p}{v_{pb}} \left(\frac{1}{\beta_b m_b v_p v_{pb}} + 1 \right) \right] \times \exp\left(-\frac{1}{2}\beta_b m_b (v_p + v_{pb})^2\right) \right\} \times \left\{ 2\text{Re}\Psi(1 + i\eta_{pb}) - \ln \eta_{pb}^2 \right\}, \quad (12)$$

where $\Psi(z)$ is the logarithmic derivative of the gamma function. Finally, the total stopping power can be expressed as

$$\frac{dE}{ds} = \frac{dE^{NI}}{ds} + \frac{dE^{\text{Coul}}}{ds}. \quad (13)$$

This equation defines the energy loss of the projectile p to the plasma particles of species b or, equivalently, the energy *gain* of the plasma particles b brought about by the projectile p moving through the plasma with the velocity v_p.

III. RANGE AND PENETRATION DEPTH

For two-body elastic collision, the particles' velocities before and after the collision are considered as $\mathbf{v}_p$, $\mathbf{v}_b$ and $\mathbf{v}'_p$, $\mathbf{v}'_b$, respectively. The Boltzmann equation for the distribution function $f_p(\mathbf{p}_p)$ of charged particles p is written as [23]

$$\left[\frac{\partial}{\partial s} + \hat{\Omega}.\nabla\right] f_p(\mathbf{r},\mathbf{p}_p,s) = \int \frac{d^3\mathbf{p}_b}{(2\pi\hbar)^3} \int [f_b(\mathbf{p}'_b) f_p(\mathbf{p}'_p) - f_b(\mathbf{p}_b) f_p(\mathbf{p}_p)] \frac{d\sigma_{pb}}{d\Omega} d\Omega, \quad (14)$$

where $\hat{\Omega}$ is the unit vector for directing the motion of the projectile p. This relation describes the scattering of the particles of mass m_p and m_b, the scattering from the initial momenta $\mathbf{p}_p = m_p\mathbf{v}_p$, $\mathbf{p}_b = m_b\mathbf{v}_b$ to the final momenta $\mathbf{p}'_p = m_p\mathbf{v}'_p$, $\mathbf{p}'_b = m_b\mathbf{v}'_b$. If the background plasma species b are assumed to be stationary ($v_b = 0$), such as a cold matter, Eq. (14) is converted to the diffusion equation

$$\left[\frac{\partial}{\partial s} + \hat{\Omega}.\nabla\right] f_p(\mathbf{r},\mathbf{p}_p,s) = n_b \int [f_p(\mathbf{p}'_p) - f_p(\mathbf{p}_p)] \frac{d\sigma_{pb}}{d\Omega} d\Omega, \quad (15)$$

where n_b is the number density of background component b. Equation (15) is solved in a cylindrical coordinate with the assumption that the scattering is azimuthally symmetric. The solution that satisfies the boundary conditions for projectile angular distribution is [11,12]

$$f_p(\theta,E) = \frac{1}{4\pi} \sum_{\ell=0}^{\infty} P_\ell(\cos\theta) \times \exp\left[-\int_E^{E_0} k_\ell(E') \left(\frac{dE'}{ds}\right)^{-1} dE' \right], \quad (16)$$

where $P_\ell(\cos\theta)$ are the Legendre polynomials. Using orthogonality, the average values of the Legendre polynomials take simple expressions

$$\langle P_\ell(\cos\theta)\rangle = \exp\left[-\int_E^{E_0} k_\ell(E') \left(\frac{dE'}{ds}\right)^{-1} dE' \right]. \quad (17)$$

The effects of the scattering are manifested by the macroscopic transport cross sections of various orders (ℓ) which are all functions of the energy loss

$$k_\ell(E) = \sum_b n_b \int \frac{d\sigma_{pb}}{d\Omega} [1 - P_\ell(\cos\theta)] d\Omega. \quad (18)$$

As mentioned above, Eqs. (16) through (18) are obtained from diffusion equation (15) assuming cold matter ($v_b = 0$). However, this assumption is not appropriate for the warm dense matter such as the central high density region of fast ignition fusion targets. One of the good approximations for such plasmas is considering the plasma component b to be in thermal equilibrium with the Maxwellian distribution function

$$f_b(\mathbf{p}_b) = n_b \left(\frac{2\pi\hbar^2\beta_b}{m_b}\right)^{3/2} \exp\left(-\frac{1}{2}\beta_b m_b v_b^2\right). \quad (19)$$

To find a suitable solution, we refer to the Boltzmann equation (14) and assume that the distribution function of the background plasma component b does not change by the

scattering $[f_b(\mathbf{p}'_b) \simeq f_b(\mathbf{p}_b)]$. The solution is straightforward and helps us to evaluate the transport cross sections $k_\ell(E)$, in particular, when $\ell = 1$

$$k_1^{\mathrm{Coul},NI}(E) = \sum_b \int \frac{d^3\mathbf{p}_b}{(2\pi\hbar)^3} f_b(\mathbf{p}_b) \int \frac{d\sigma_{pb}^{\mathrm{Coul},NI}}{d\Omega}(1-\cos\theta)d\Omega, \tag{20}$$

where $k_1(E) = k_1^{\mathrm{Coul}}(E) + k_1^{NI}(E)$.

Since differential cross sections are evaluated in the center-of-mass coordinate, the second integration of Eq. (20) may be performed by passing to the center-of-mass coordinate

$$\left(\frac{d\sigma}{d\Omega}\right)^L \sin\theta d\theta = \left(\frac{d\sigma}{d\Omega}\right)^{CM} \sin\Theta d\Theta, \tag{21}$$

and the scattering angle in laboratory coordinate θ is related to the scattering angle in the center-of-mass coordinate Θ as

$$\cos\theta = \frac{\left(v_p^c\right)^2 \cos\Theta + \mathbf{v}_p^c.\mathbf{V} + v_p^c V\{\cos\alpha\cos\Theta - \sin\alpha\sin\Theta\} + V^2}{v_p\left[\left(v_p^c\right)^2 + V^2 + 2v_p^c V\{\cos\alpha\cos\Theta - \sin\alpha\sin\Theta\}^{1/2}\right]}, \tag{22}$$

where α is the angle between $\mathbf{v}_p^c$ and $\mathbf{V}$

$$\cos\alpha = \frac{\mathbf{v}_p^c.\mathbf{V}}{v_p^c V}, \tag{23}$$

and

$$\mathbf{v}_p^c = \frac{m_b}{M_{pb}}(\mathbf{v}_p - \mathbf{v}_b), \tag{24}$$

is the projectile velocity in the center-of-mass system and

$$\mathbf{V} = \frac{m_p\mathbf{v}_p + m_b\mathbf{v}_b}{M_{pb}}, \tag{25}$$

is the velocity of center of mass. For an elastic Coulomb collision, the relation scattering angle in the center-of-mass coordinate Θ with the impact parameter τ is

$$\cot\frac{\Theta}{2} = \frac{\tau}{\zeta}; \quad \zeta = \frac{Z_p Z_b e^2}{m_{pb} v_{pb}^2}. \tag{26}$$

The Coulomb cross section diverges logarithmically in both the short- and long-distance regimes. To obtain a finite result, we must introduce the short- and long-distance cutoffs $\tau_{\min}$ and $\tau_{\max}$ as we integrate over the impact parameter τ. Equations (1) and (22) are substituted into Eq. (20) and, after a standard change of variables Eq. (26) the Coulomb component is obtained

$$\begin{aligned} k_1^{\mathrm{Coul}}(E) = {} & \sum_b n_b (2\pi)^{1/2} (m_b\beta_b)^{3/2} \int_0^\infty dv_b v_b^2 \\ & \times \exp\left\{-\frac{1}{2}m_b\beta_b v_b^2\right\} \int_0^\pi \sin\vartheta d\vartheta \\ & \times \int_{\tau_{\min}}^{\tau_{\max}} \tau d\tau \left\{1 - \frac{\frac{\chi(\tau^2-\zeta^2)}{\tau^2+\zeta^2} - \frac{2\xi\tau\zeta}{\tau^2+\zeta^2} + \nu}{v_p\left[u + \frac{2\omega(\tau^2-\zeta^2)}{\tau^2+\zeta^2} - \frac{4\xi\tau\zeta}{\tau^2+\zeta^2}\right]^{1/2}}\right\}, \end{aligned} \tag{27}$$

where the variables are defined as

$$\begin{aligned} \omega &= v_p^c V\cos\alpha, \\ \chi &= \left(v_p^c\right)^2 + v_p^c V\cos\alpha, \\ \xi &= v_p^c V\sin\alpha, \\ \nu &= \mathbf{v}_p^c.\mathbf{V} + V^2, \\ u &= \left(v_p^c\right)^2 + V^2. \end{aligned} \tag{28}$$

The Debye screening sets the scale for the long-distance cutoff and we expect on physical grounds that $\tau_{\max} = k_D^{-1}$. The short-distance cutoff is set by interpolation between the extreme quantum and classical regimes $\tau_{\min} = \sqrt{\zeta^2 + (\hbar/2m_{pb}v_{pb})^2}$ [24]. As a result, from Eq. (17) we can obtain

$$\langle\cos\theta\rangle = \exp\left[-\int_E^{E_0} k_1(E')\left(\frac{dE'}{ds}\right)^{-1} dE'\right], \tag{29}$$

where $\cos\theta$, a function of the residual proton energy E and the initial energy E_0, is a measure of the mean deflection resulting from multiple scattering. Equations (13) and (29) can be used to calculate the stopping power in the direction of the initial projectile velocity

$$\frac{dE}{dx} = \langle\cos\theta\rangle^{-1}\frac{dE}{ds}, \tag{30}$$

where dE/ds is the stopping power along the path while dE/dx is the linear energy stopping power. It can be noticed, however, that the computation of the range (i.e., the length of the projectile trajectory) does not require the consideration of scattering and can also be performed by numerically integrating the equation

$$R = \int_E^{E_0}\left(\frac{dE'}{ds}\right)^{-1} dE' \tag{31}$$

by using the linear energy deposition (30), which can be evaluated

$$\langle x\rangle = \int_E^{E_0}\langle\cos\theta\rangle\left(\frac{dE'}{ds}\right)^{-1} dE'. \tag{32}$$

$\langle x\rangle$ is the mean longitudinal projectile position, by starting energy E_0, and travels to be slowed down to reach the energy E, which is named penetration depth.

IV. RESULTS AND DISCUSSIONS

According to Atzeni's model, the minimum ignitor beam energy, power, and intensity required for FI are affected by the proton stopping range ρr over the interval $0.15 < \rho r < 1.2\,\mathrm{g\,cm^{-2}}$, where ρr is the hot spot diameter at the proton beam transport direction [25]. Further studies show that for high gain FI, the assembled fuel should be compressed to a mass density in the range $\rho = 300$–$500\,\mathrm{g\,cm^{-3}}$ to keep the required ignition energy and the fusion yield at manageably

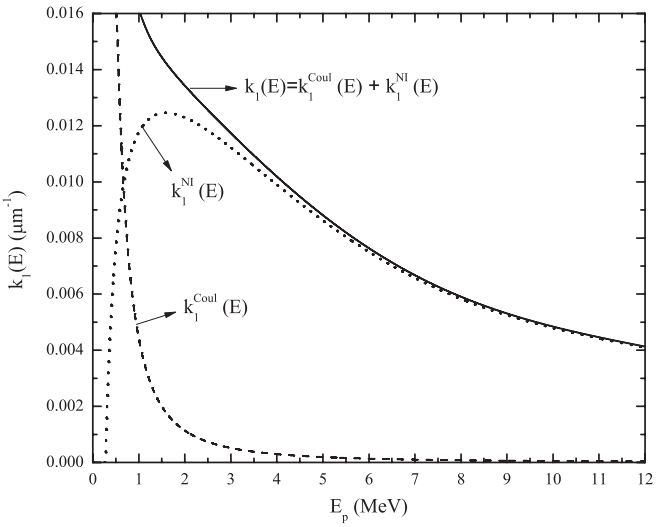

FIG. 2. The transport cross section Eq. (20) for 0.1–12 MeV protons in a uniform D/T plasma with $\rho = 300\,\mathrm{g\,cm^{-3}}$ and $T = 5$ keV. The contributions of Coulomb (dashed line) and nuclear elastic (dotted line) scattering are shown.

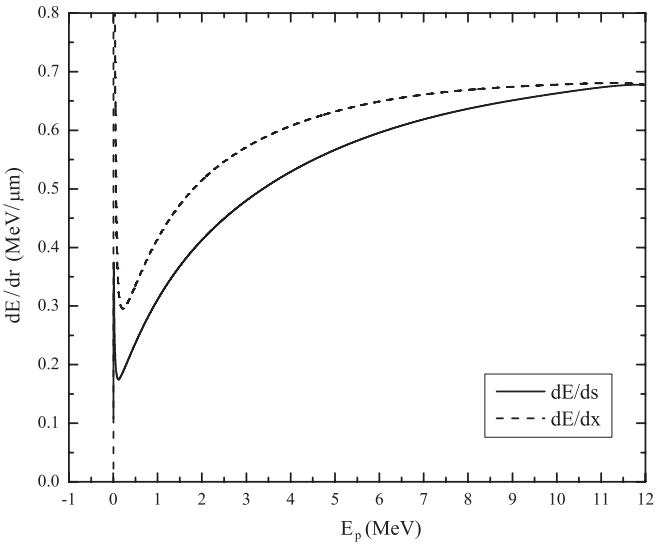

FIG. 4. Stopping power for linear energy transfer and continuous slowing down as a function of the proton energy for incident 12 MeV protons in a uniform D/T plasma $\rho = 500\,\mathrm{g\,cm^{-3}}$, $T = 5$ keV.

small levels [26]. The initially compressed inertial confinement fusion target temperature is typically found to be $\sim$1 keV, while complete burn propagation requires that the hot spot reaches an average temperature $T = 5$–10 keV. Moreover, the proton beam should deposit its energy in the fuel within 10–20 ps, before it hydrodynamically disassembles to isochorically heat the "hot spot" to ignition temperature. For comparison, we calculated the proton stopping time using the following equation:

$$t_{\mathrm{dep}} = \int_{E_{\mathrm{th}}}^{E_0} \left(\frac{dE'}{dt}\right)^{-1} dE', \tag{33}$$

where E_{th} is the thermal energy. The results in Fig. 1 show that the stopping time, although sensitive to the proton initial energy, fuel density, and temperature, is not a major concern here as it be stopped within $t_{\mathrm{dep}} \lesssim 4$ ps at the energies up to 12 MeV. As a result, it can be assumed that the protons deposit their energy in a precompressed DT fuel that is initially at rest because the fuel is almost stagnated at the time of peak ρr.

The transport cross section was calculated using Eq. (20). The results are plotted in Fig. 2. For $E_p \gtrsim 1$ MeV, nuclear elastic scattering of protons with plasma ions is the main contribution of the transport cross section. Calculating Eq. (29), Fig. 3 illustrates the circumstance when the incident proton ($E_0 = 12$ MeV) continuously changes direction as it loses energy. Densities $\rho = 300{,}500\ \mathrm{g\,cm^{-3}}$ and temperatures $T = 5{,}10$ keV are chosen to be relevant to the compressed targets of fast ignition in ignition condition. This figure shows

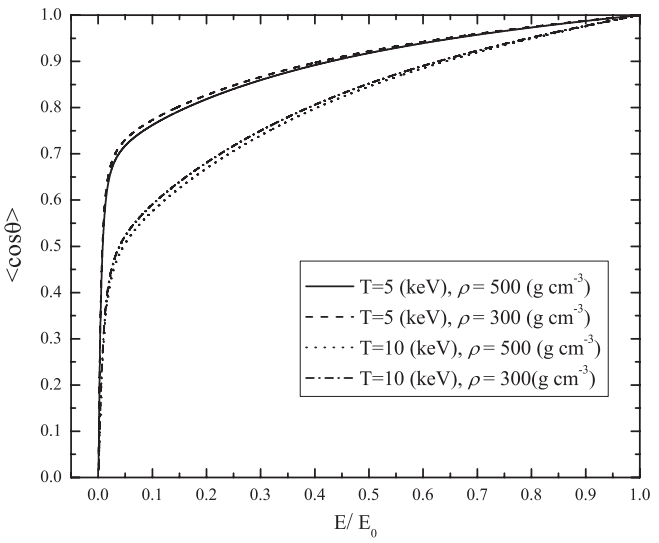

FIG. 3. The mean deflection angle $\langle\cos\theta\rangle$ versus the fraction of the residual energy in a uniform D/T plasma for 12 MeV protons with $\rho = 300{,}500\,\mathrm{g\,cm^{-3}}$ and $T = 5{,}10$ keV.

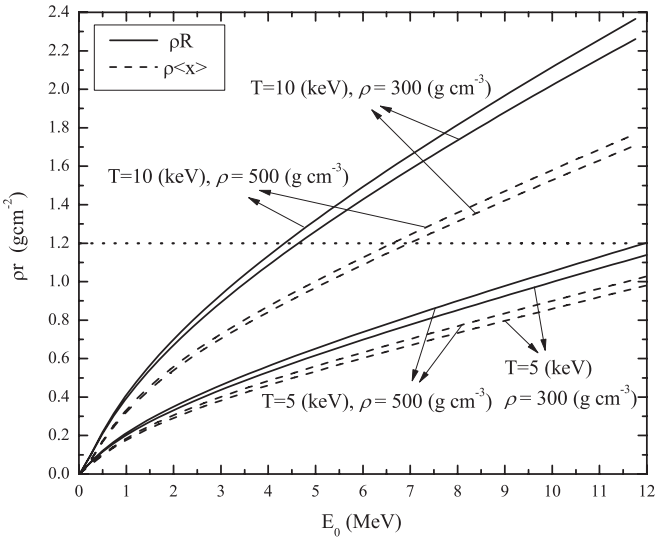

FIG. 5. The range (solid line) and penetration (dashed line) for 2–12 MeV protons in a uniform D/T plasma with $\rho = 300{,}500\,\mathrm{g\,cm^{-3}}$ and $T = 5{,}10$ keV.

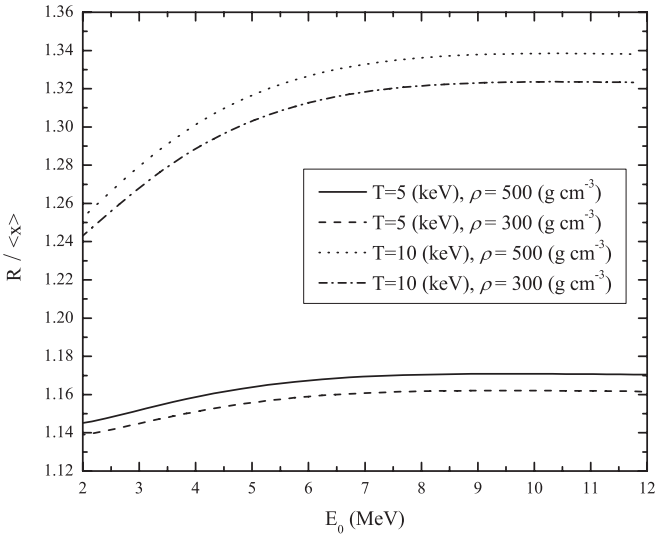

FIG. 6. The ratio of range to penetration for 2–12 MeV protons in a uniform D/T plasma with $\rho = 300,500\,\mathrm{g\,cm^{-3}}$ and $T = 5,10$ keV.

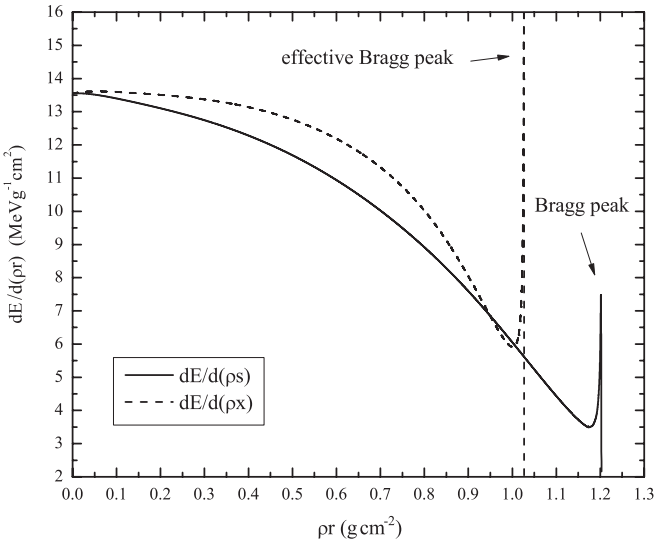

FIG. 7. The stopping power for 12 MeV protons, as a function of the proton penetration, for a uniform D/T plasma with $\rho = 500\,\mathrm{g\,cm^{-3}}$ and $T = 5$ keV.

that by increasing the density at the mean deflection angle does not change effectively, and it is more sensible than temperature. Increasing the temperature leads to an increase in the mean deflection angle due to multiple scattering. This figure also shows that the near-thermalized energy scattering mainly leads to deflect the beam from the initial direction. For example, for $\rho = 300\,\mathrm{g\,cm^{-3}}$ and $T = 5$ keV, when $E/E_0 \approx 0.01$ the mean deflection angle is $|\theta| \approx 56^\circ$, at which point the incident proton has lost the memory of its initial direction.

By substituting this result in Eq. (30), Fig. 4 illustrates the stopping power for linear transfer and continuous slowing down as a function of the proton energy, for $\rho = 500\,\mathrm{g\,cm^{-3}}$, $T = 5$ keV. The enhancement of dE/dx (dashed lines) over dE/ds (solid line) is a consequence of the effects of multiple scattering.

Figure 5 plots the range ρR and the penetration depth $\rho\langle x\rangle$ that the proton traverses as it scatters about and eventually thermalizes, as a function of the initial proton energy. This figure also shows dependences of the range and penetration depth to the target density and temperature. The results in Fig. 5 show that, at lower hot spot temperature ($T = 5$ keV), 12 MeV protons can deposit their energy into the hot spot at $\rho r < 1.2\,\mathrm{g\,cm^{-2}}$. However, when the hot spot becomes even hotter to $T = 10$ keV, the desired proton's initial energy decreases to $\lesssim$6.5 MeV to meet the optimal deposition depth requirement. For further comparison, the ratio of range to penetration is depicted in Fig. 6, for 2–12 MeV protons in a uniform D/T plasma with $\rho = 300,500\,\mathrm{g\,cm^{-3}}$ and $T = 5,10$ keV. As the initial proton energy, temperature, and density increase, the effects of multiple scattering becomes more pronounced, and the penetration is further diminished with respect to the range.

With the calculation of the penetration as a function of energy loss, the linear energy deposition can be evaluated (Fig. 7). In addition to the differences in total penetration with and without scattering contributions, it is seen that the linear energy transfer increases near the end of its penetration (i.e., an effective Bragg peak). Such differences may need to be considered in quantitatively modeling the energy deposition of protons for fast ignition, and for critically assessing ignition requirements. In summary, the mean deflection angle, energy loss, range, and penetration of multi-megaelectron volt protons into a uniform deuterium-tritium plasma has been calculated, and the effects of multiple scattering such as Coulomb and nuclear elastic scattering is treated from a unified point of view. The plasma conditions ($\rho = 300,500\,\mathrm{g\,cm^{-3}}$ and $T = 5,10$ keV) are chosen to be relevant to compressed targets of fast ignition in ignition condition. Also, plasma components (ions and electrons) are assumed to be in thermal equilibrium with the Maxwellian distribution function. In general, scattering enhances the proton linear-energy transfer along the initial proton direction and reduces the proton penetration. Energy deposition increases near the end of its range. These results should have relevance to proton fast ignition and to proton radiography in inertial confinement fusion, specifically to energy deposition calculations that critically assess quantitative ignition requirements.

[1] G. N. Basov, S. Guskov, and L. P. Feokistov, J. Sov. Laser Res. **13**, 399 (1992).

[2] M. Tabak, J. Hammer, M. E. Glinsky, W. L. Kruer, S. C. Wilks, J. Woodworth, E. M. Campbell, M. D. Perry, and J. R. Mason, Phys. Plasmas **1**, 1626 (1994).

[3] B. Qiao, M. Zepf, M. Borghesi, and M. Geissler, Phys. Rev. Lett. **102**, 145002 (2009).

[4] J. Badziak, G. Mishra, N. K. Gupta, and A. R. Holkundkar, Phys. Plasmas **18**, 053108 (2011).

[5] R. A. Snavely *et al.*, Phys. Rev. Lett. **85**, 2945 (2000).

[6] M. Roth *et al.*, Phys. Rev. Lett. **86**, 436 (2001).
[7] L. Volpe *et al.*, Phys. Plasmas **18**, 012704 (2011).
[8] C. Deutsch, H. Furukawa, K. Mima, M. Murakami, and K. Nishihara, Phys. Rev. Lett. **77**, 2483 (1996); **85**, 1140(E) (2000).
[9] C. K. Li and R. D. Petrasso, Phys. Rev. E **70**, 067401 (2004).
[10] C. K. Li and R. D. Petrasso, Phys. Rev. E **73**, 016402 (2006); Phys. Plasmas **13**, 056314 (2006).
[11] S. A. Goudsmit *et al.*, Phys. Rev. **57**, 24 (1940).
[12] H. W. Lewis, Phys. Rev. **78**, 526 (1950).
[13] M. Mahdavi and T. Koohrokhi, Mod. Phys. Lett. A **26**, 1561 (2011).
[14] L. Yin, B. J. Albright, B. M. Hegelich, K. J. Bowers, K. A. Flippo, T. J. T. Kwan, and J. C. Fernandez, Phys. Plasmas **14**, 056706 (2007).
[15] R. Betti, A. A. Solodov, J. A. Delettrez, and C. Zhou, Phys. Plasmas **13**, 100703 (2006).
[16] S. Atzeni, A. Schiavi, and C. Bellei, Phys. Plasmas **14**, 052702 (2007).
[17] M. Temporal, J. J. Honrubia, and S. Atzeni, Phys. Plasmas **15**, 052702 (2008).
[18] A. Andrade and G. M. Hale, Phys. Rev. A **30**, 1940 (1984).
[19] L. S. Brown, D. L. Preston, and R. L. Singleton Jr., Phys. Rep. **410**, 237 (2005).
[20] R. Balescu, Phys. Fluids **3**, 52 (1960).
[21] K. Morawetz, Phys. Rev. E **50**, 4625 (1994).
[22] K. Morawetz and G. Röpke, Phys. Rev. E **54**, 4134 (1996).
[23] D. Kremp, M. Schlanges, and W.-D. Kraeft, *Quantum Statistics of Nonideal Plasmas* (Berlin, Springer, 2005).
[24] C. K. Li and R. D. Petrasso, Phys. Rev. Lett. **70**, 3063 (1993).
[25] S. Atzeni, Phys. Plasmas **6**, 3316 (1999).
[26] J. C. Fernandez, B. J. Albright, K. A. Flippo, B. M. Hegelich, T. J. Kwan, M. J. Schmitt, and L. Yin, J. Phys.: Conf. Ser. **2**, 022051 (2008).